Geochemistry Geophysics Geosystems G3
AN ELECTRONIC JOURNAL OF THE EARTH SCIENCES
Published by AGU and the Geochemical Society

Article
Volume 2
October 16, 2001
Paper number 2000GC000136
ISSN: 1525-2027

Variation of cooling rate with depth in lower crust formed at an oceanic spreading ridge: Plagioclase crystal size distributions in gabbros from the Oman ophiolite

Carlos J. Garrido
Woods Hole Oceanographic Institution, Department of Geology and Geophysics, Woods Hole, Massachusetts, USA

Now at Instituto Andaluz de Ciencias de la Tierra (IACT), CSIC and Universidad de Granada, Facultad de Ciencias, Fuentenueva s/n, 18002 Granada, Spain. (carlosg@ugr.es)

Peter B. Kelemen and Greg Hirth
Woods Hole Oceanographic Institution, Department of Geology and Geophysics, Woods Hole, Massachusetts, USA

[1] **Abstract:** Analysis of crystal size distributions (CSD) of plagioclase in gabbros from the Oman ophiolite indicates that cooling rates in the lower crust beneath a medium- to fast-spreading oceanic ridge did not vary smoothly with depth. Cooling rates in the upper half of the gabbro section were approximately 1.5–2 times faster than in the lower half of the gabbro section during igneous crystallization and/or high temperature grain growth processes. Our results are inconsistent with thermal models for oceanic spreading ridges that approximate the effect of hydrothermal convection by using an enhanced thermal conductivity together with a conductive heat transfer mechanism. Instead, the Oman CSD data are consistent with recent seismic and modeling studies that suggest that hydrothermal convection leads to closely spaced, near-vertical isotherms in the upper half of the plutonic section within a few kilometers of the ridge axis.

Keywords: Mid-ocean ridges; oceanic crust accretion; plagioclase crystal size distribution; oceanic gabbros; Oman ophiolite.

Index terms: Mid-ocean ridge processes; oceanic crust; igneous petrology; heat flow (benthic) and hydrothermal processes.

Received December 15, 2000; **Revised** July 5, 2001; **Accepted** July 6, 2001; **Published** October 16, 2001.

Garrido, C. J., P. B. Kelemen, and G. Hirth, 2001. Variation of cooling rate with depth in lower crust formed at an oceanic spreading ridge: Plagioclase crystal size distributions in gabbros from the Oman ophiolite, *Geochem. Geophys. Geosyst.*, *2*, 10.1029/2000GC000136, 2001.

1. Introduction

[2] The crystal size distribution (CSD) of plagioclase may contain a record of conditions during solidification and high-temperature deformation [*Cashman and Marsh*, 1988; *Marsh*, 1988; *Cashman*, 1990; *Higgins*, 1998; *Marsh*, 1998]. Here we present a study of

Copyright 2001 by the American Geophysical Union

plagioclase CSDs in a suite of gabbros from the lower crustal section of the Oman ophiolite aimed at constraining the thermal conditions of crystallization of the plutonic crust at medium- to fast-spreading mid-ocean ridges. Several parameters of plagioclase CSD plots in the Oman gabbro section display a "stepped" spatial distribution. Less than 2 km above the Moho Transition Zone (MTZ), gabbros have plagioclase CSD plots with steeper slopes and larger intercepts than gabbros more than 2 km above the MTZ. This distribution is consistent with faster cooling and crystallization of the upper half of the gabbros relative to the lower half. Faster solidification of the upper half of the plutonic section can be caused by near-axis hydrothermal convection.

[3] These results are at odds with theoretical studies in which the effect of hydrothermal circulation is modeled using an enhanced thermal conductivity, together with a conductive heat transport mechanism, producing a modified, conductive geotherm and a gradual decrease in cooling rate with depth in the plutonic oceanic crust [*Sleep*, 1975; *Phipps Morgan and Chen*, 1993; *Chevenez et al.*, 1998]. We infer that heat is efficiently extracted from the lower oceanic crust by deep, near-axis hydrothermal convection, producing near-vertical isotherms in the cooling plutonic crust, as recently modeled by *Cherkaoui et al.* [1999]. Similarly, results of recent seismic tomography studies of the lower oceanic crust at the East Pacific Rise are consistent with the presence of near-vertical isotherms resulting from hydrothermal circulation [*Dunn et al.*, 2000].

[4] The Oman ophiolite is one of the best exposed sections of igneous crust formed at an oceanic spreading center. Because the crustal section includes a continuous layer of gabbro overlain by sheeted dikes, which in turn are overlain by pillow basalts, it is clear that most of the igneous rocks of this ophiolite formed at a fast- to medium-spreading ridge similar to the East Pacific Rise or the Juan de Fuca Ridge [*Nicolas*, 1989; *Nicolas et al.*, 1996]. Our study focused on a suite of 16 gabbros from a 4.5 km thick lower crustal section in the Wadi Tayin massif, near the locality of Khafifah, extending from the MTZ to the sheeted-dike transition (Figure 1). Whole-rock major and trace element compositions are shown as a function of the distance from the MTZ in Figure 2. These and other data indicate that the gabbros were comagmatic and were in trace element exchange equilibrium with melts similar to normal mid-ocean ridge basalt and with sheeted dikes and lavas of the Oman ophiolite [*Pallister and Knight*, 1981; *Kelemen et al.*, 1997]. Notable exceptions are the gabbro samples from the uppermost kilometer of the section, which display higher Na_2O and La contents and highly variable anorthite contents in plagioclase (Figure 2). These high La compositions probably reflect a higher proportion of "trapped melt" during solidification of these samples [*Kelemen et al.*, 1997; *Korenaga and Kelemen*, 1998].

[5] Much has been written about the tectonic setting of the Oman spreading ridge (arc, back arc, mid-ocean ridge, etc.). Readers should be aware that all discussions based on the trace element composition of lavas [e.g., *Pearce et al.*, 1981] have been based on samples from the northwestern massifs of the ophiolite, where andesites and dacites are common in both "lower" and "upper" lavas. In this study we have focused on the Wadi Tayin area, the southeasternmost massif in the ophiolite. Only basaltic lavas with flat rare earth patterns, indistinguishable in both major and trace element contents from mid-ocean ridge basalts, are known in this massif [*Pallister and Hopson*, 1981; *Pallister and Knight*, 1981]. Thus, although one cannot rule out an origin in, e.g., a back arc, it is clear that processes beneath the Oman spreading center produced basaltic magmas similar to mid-ocean ridge basalts.

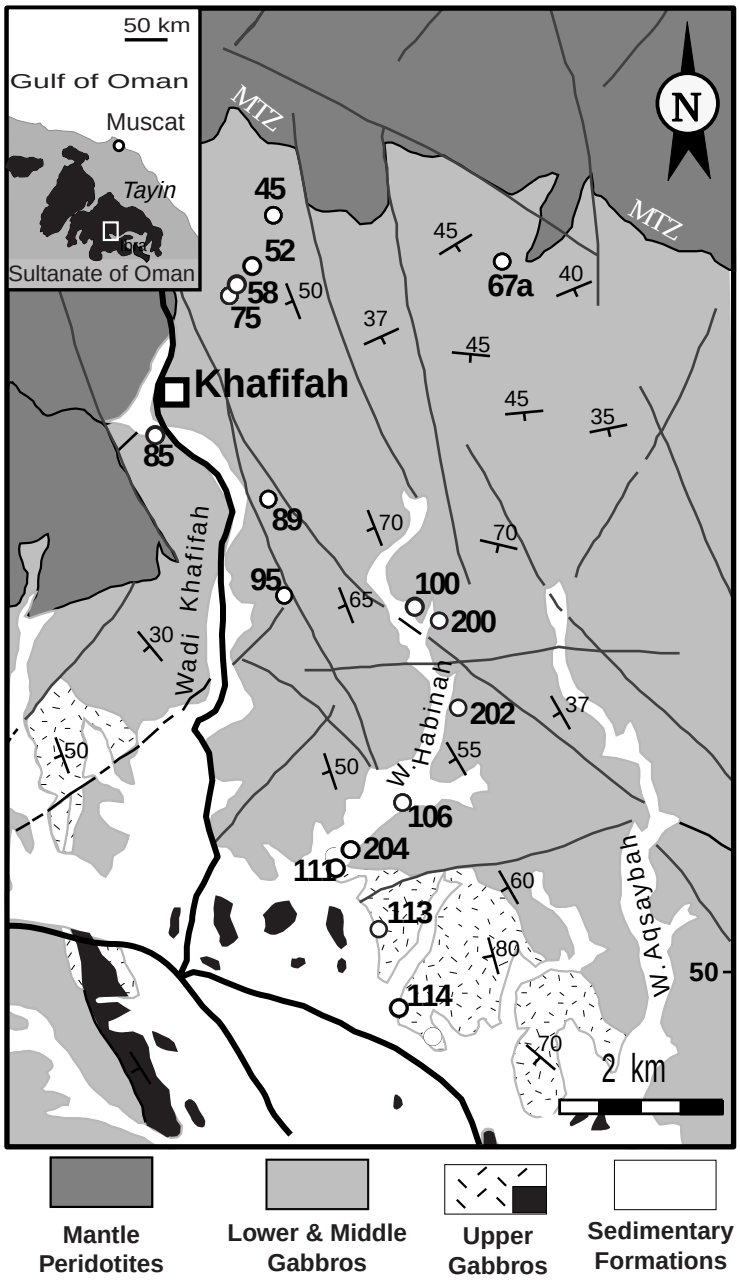

Figure 1. Simplified geological map of the Khafifah section of the Wadi Tayin massif (Oman ophiolite, Sultanate of Oman) [after *Hopson et al.*, 1981] showing the locations of our samples. The inset shows the location of the study area (white rectangle) within the eastern part of the Oman ophiolite. The orientation of modal banding in the gabbros is shown using strike and dip symbols.

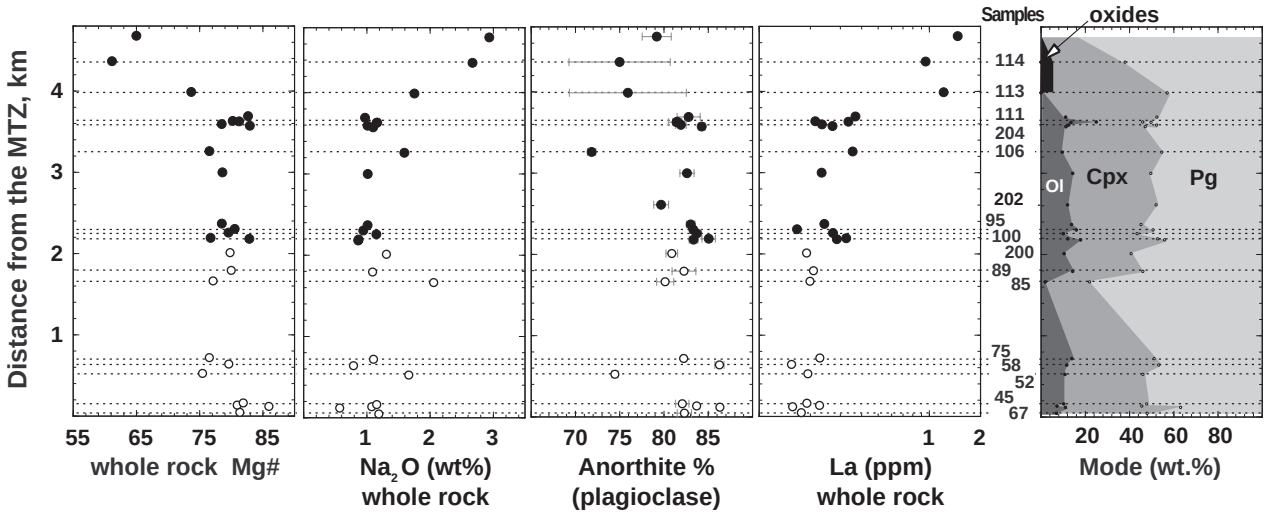

Figure 2. Modal, whole-rock, and mineralogical compositional variations in gabbros from the Khafifah section as a function of distance from the Moho Transition Zone (MTZ). Dashed lines indicate the samples selected for our crystal size distribution (CSD) study. Modal variations were computed by inversion of whole-rock and mineral major element data (P. B. Kelemen and C. J. Garrido, manuscript in preparation, 2001). Chemical analyses were conducted on the same sample chips as the thin sections used for determining plagioclase CSDs.

2. Methods

[6] Plagioclase CSDs were determined using the following procedure. We made large thin sections perpendicular to mineral layering and/or foliation in all cases and parallel to mineral lineation where it was observed. A plane light digital image was used to identify mafic minerals and estimate the modal proportion of plagioclase. For representative areas in each thin section, a binary image of plagioclase grain boundaries was generated by image-processing procedures combining several photomicrographs taken in cross-polarized light at different polarizer positions. Perfect registration of sequential images was obtained by building a microscope stage in which polarizers rotated together while the sample and camera remained fixed. Binary images were manually edited to correct for artificial crystal outlines. Examples of photomicrographs and the resulting plagioclase grain boundary digital images are shown in Figure 3.

[7] The binary image of plagioclase grain boundaries, without mafic minerals, was used to measure plagioclase crystal section areas, lengths, and widths using commercial image processing software. From these two-dimensional (2-D) data the number of crystals per mm^3 as a function of size was estimated using the stereological procedure proposed by *Higgins* [2000b] together with his CSD correction software (available at http://wwwdsa.uqac.uquebec.ca/~mhiggins/csdcorrections.html). Three important parameters must be specified as input in this procedure: (1) the average 3-D aspect ratio of the plagioclase crystals, (2) the characteristic size parameter used in the transformation (i.e., apparent 2-D widths or lengths) [*Peterson*, 1996; *Sahagian and Proussevitch*, 1998; *Higgins*, 2000b], and (3) the degree of lineation.

[8] We estimated the average three-dimensional aspect ratio of plagioclase from the width-length distribution of 2-D plagioclase profiles in thin section using a procedure modified from *Higgins* [1994]. The mean 3-D ratio of the intermediate to short axis can be estimated from the mode of the distribution of the 2-D width/length ratios [*Higgins*, 1994]. We found that the method recommended by *Higgins* [1994] does not accurately predict the longest dimension of crystals in three dimensions. Therefore we conducted a Monte Carlo simulation using 10^5 random cuts through synthetic parallelepipeds with specified aspect ratios. Then, given a 3-D intermediate/short axis ratio, we found that the 3-D intermediate/long axis ratio can be estimated using the mean of the 2-D width/length ratios as shown in Figure 4. The mean 3-D aspect ratios of plagioclase determined in this fashion (reported for each sample in the bottom of the CSD plots in Figure 5) were used as input to the Higgins CSD correction software.

[9] We used the 2-D widths of plagioclase sections as the characteristic size parameter in the stereological transformation. Two-dimensional width is preferable to 2-D length because, for the tabular and prismatic habits typical of plagioclase, the use of 2-D length results in spurious kinks at the larger size classes in CSD plots [*Peterson*, 1996; *Higgins*, 2000b]. Finally, we assumed that all rocks have a weak lineation. However, this assumption does not make a significant difference in the results [*Higgins*, 2000b].

3. Results

[10] The plagioclase CSDs of our samples are shown in Figure 5 in the form of conventional CSD plots [*Marsh*, 1988]. The CSD plot is a plot of binned crystal size (L, mm) versus the natural logarithm of the crystal population density ($\ln(n)$) of each size bin [*Marsh*, 1988]. The population density (n, mm^{-4}) is the number of crystals per volume in any size

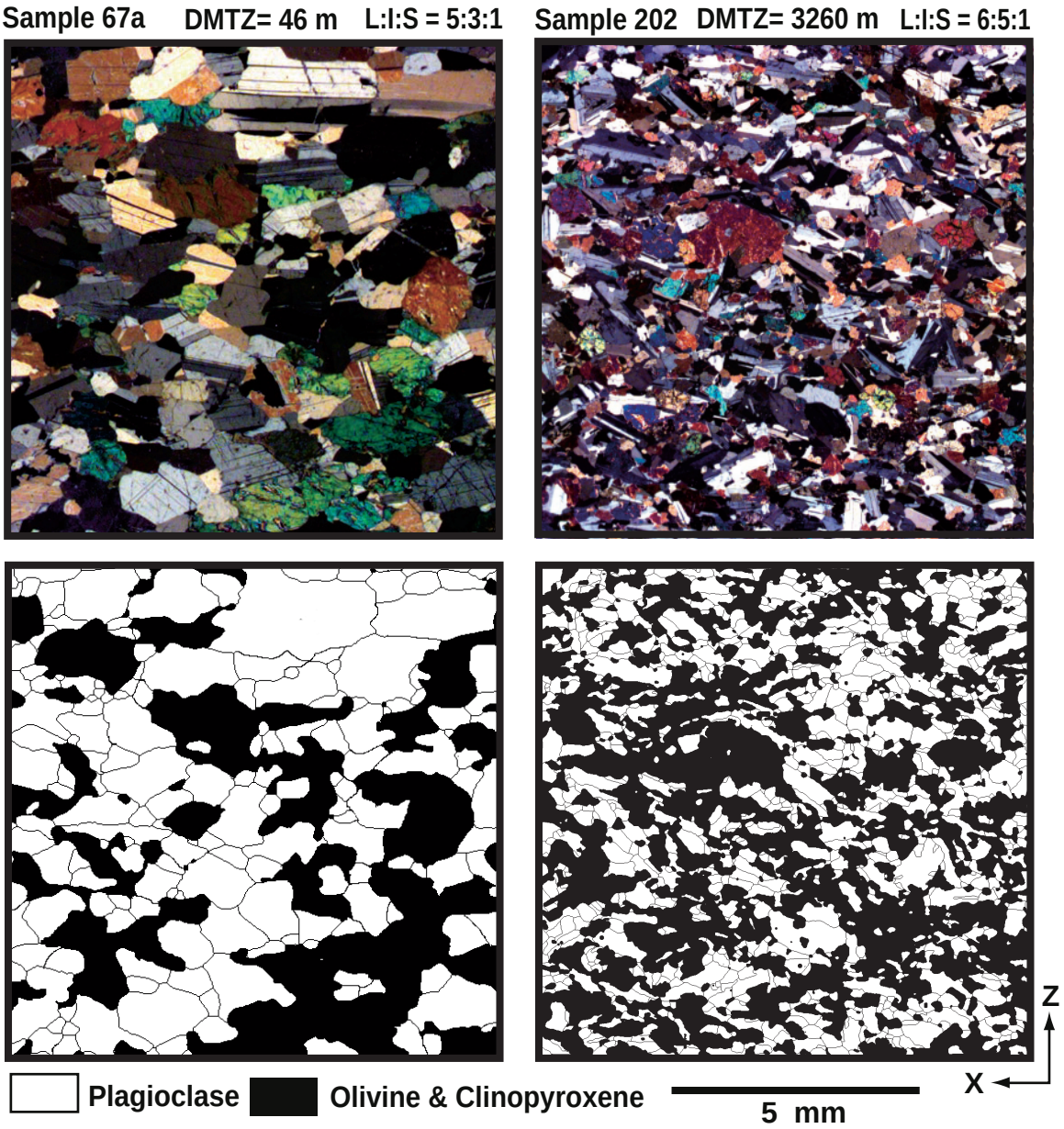

Figure 3. Photomicrographs with cross-polarized light comparing textures in gabbros from the lower (OM97-67a) and upper (OM97-202) levels of the Khafifah gabbro section. Also shown are digital, plagioclase grain boundary images of the same samples (grain boundaries are indicated by thin black lines). The thin sections are perpendicular to the foliation plane (defined by the mineral layering) and parallel to mineral lineation. L:I:S is the mean axial ratio (longest, intermediate, and short 3-D axes normalized to the short axis) of plagioclase crystal estimated using the method further described in the text.

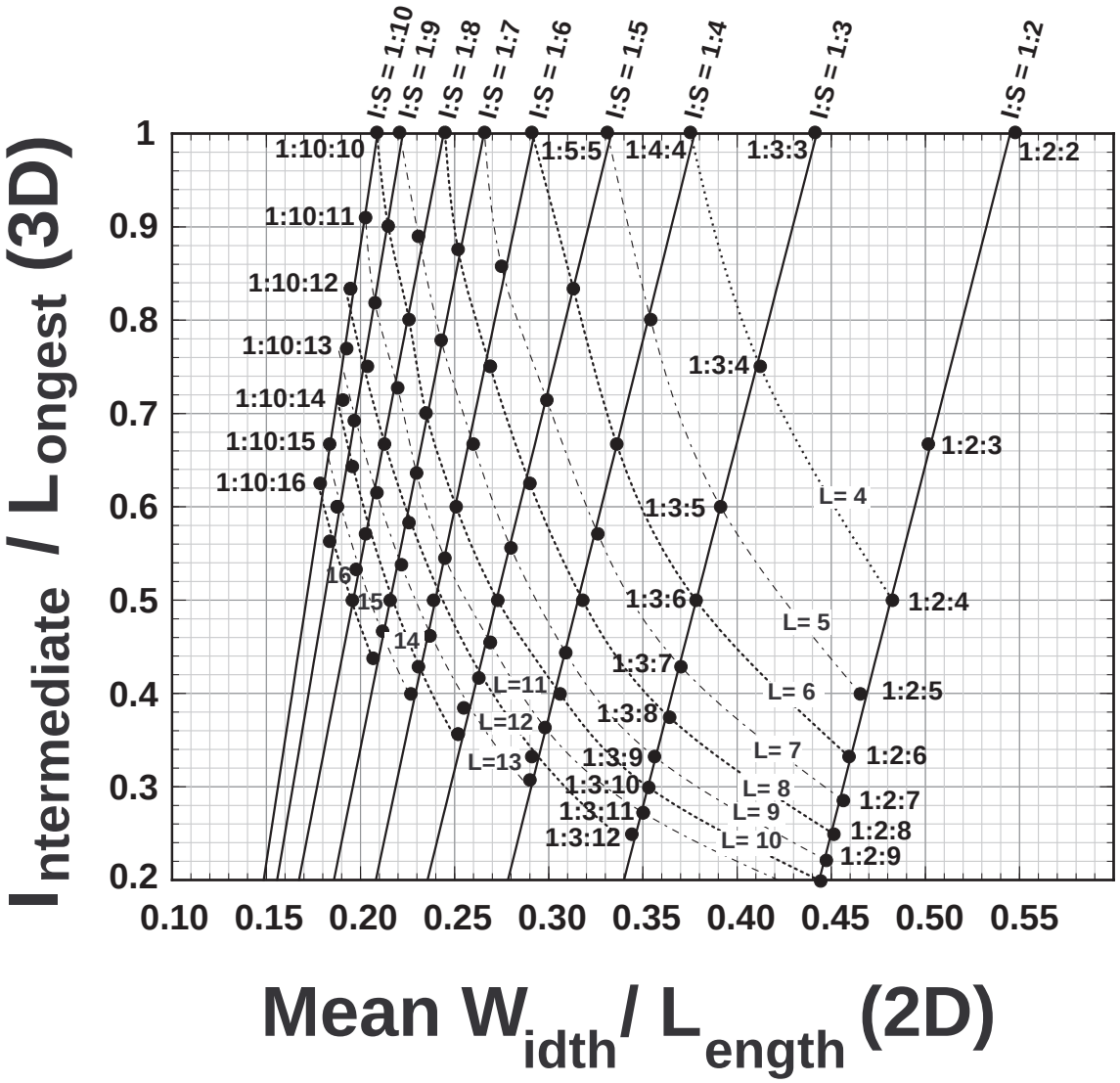

Figure 4. Ratio of intermediate (I) to long (L) dimension of plagioclase crystals in three dimensions versus ratio of mean width to length in two dimensions. Each point is based on the results of Monte Carlo simulation using 10^5 random cuts through parallelepipeds with given aspect ratios. The mean I:S ratio of the crystal in three dimensions can be estimated from the mode (most frequent value) of the 2-D width/length distribution [*Higgins*, 1994]. Given this I:S ratio (labels along the top of the grid), the mean longest dimension of crystals in three dimensions (L) can be estimated from the mean width/length observed in thin section.

bin divided by the width of the size bin [*Marsh*, 1988]. In a cumulative histogram of the number of crystals per volume versus size, the population density of the *i*th bin is the slope of the cumulative curve at the *i*th size class [*Marsh*, 1988, 1998]. The "crystal size" used in our CSD plots is the estimated 3-D crystal length computed by the CSD correction software [*Higgins*, 2000b]. All CSD plots were computed using logarithmic intervals for size. This discretization ensures a good representation of small size classes and correct sampling of

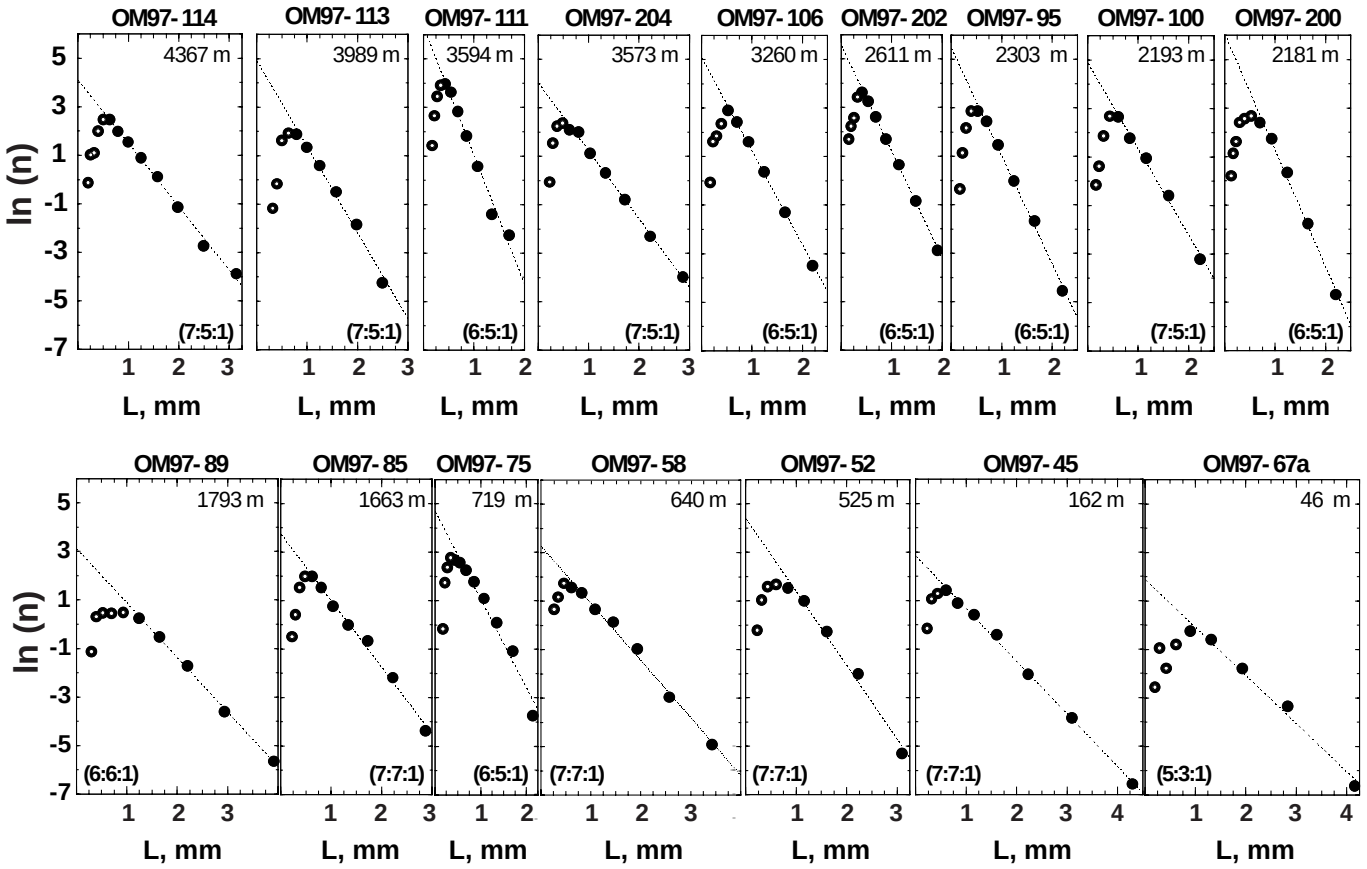

Figure 5. Plagioclase CSD plots for gabbro samples arranged in stratigraphic order. Solid symbols indicate the size classes included in the weighted-linear regressions, with the resulting fits shown by the dashed lines. In most cases the selected classes encompassed more than 80% of the measurements used to construct the CSD plot. The three-dimensional aspect ratio estimated for plagioclase using Figure 4 is given at the bottom of each plot (long:intermediate:short axis).

Table 1. Crystal Size Distribution Derived Parameters[a]

Sample	Rock Type	DMTZ, m	Slope, mm^{-1}	L_c, mm	Intercept, mm^{-4}	L_m, mm	N_v, mm^{-3}
OM97-114	gabbro	4367	−2.6 ± 0.1	0.39 ± 0.03	61 ± 5	3.1 ± 0.3	11 ± 2
OM97-113	gabbro	3989	−3.1 ± 0.1	0.32 ± 0.04	84 ± 13	2.5 ± 0.3	10 ± 1.0
OM97-111	olivine gabbro	3594	−5.4 ± 0.3	0.19 ± 0.05	612 ± 107	1.7 ± 0.2	41 ± 5
OM97-204	olivine gabbro	3573	−2.8 ± 0.2	0.36 ± 0.05	58 ± 10	2.9 ± 0.3	13 ± 2
OM97-106	olivine gabbro	3260	−3.7 ± 0.1	0.27 ± 0.04	140 ± 18	2.2 ± 0.3	17 ± 3
OM97-202	olivine gabbro	2611	−4.2 ± 0.1	0.24 ± 0.02	236 ± 18	1.9 ± 0.2	31 ± 4
OM97-95	olivine gabbro	2303	−4.1 ± 0.2	0.25 ± 0.06	173 ± 34	2.2 ± 0.3	22 ± 3
OM97-100plag	anorthosite	2193	−2.4 ± 0.1	0.42 ± 0.04	48 ± 5	3.7 ± 0.4	7 ± 1
OM97-100mafic	olivine gabbro	2193	−3.3 ± 0.2	0.31 ± 0.05	97 ± 17	2.2 ± 0.3	17 ± 2.0
OM97-200	olivine gabbro	2181	−3.6 ± 0.4	0.28 ± 0.12	123 ± 48	2.2 ± 0.3	19 ± 2
OM97-89	olivine gabbro	1793	−2.2 ± 0.1	0.46 ± 0.04	20 ± 3	3.9 ± 0.5	3.7 ± 0.5
OM97-85	olivine gabbro	1663	−2.6 ± 0.1	0.39 ± 0.06	34 ± 6	2.9 ± 0.3	12 ± 2
OM97-75	olivine gabbro	719	−3.1 ± 0.2	0.33 ± 0.06	71 ± 12	2.1 ± 0.2	18 ± 3
OM97-58plag	anorthosite	640	−1.4 ± 0.1	0.70 ± 0.08	4 ± 1	4.9 ± 0.8	2.0 ± 0.5
OM97-58mafic	olivine gabbro	640	−2.1 ± 0.1	0.47 ± 0.07	21 ± 4	3.4 ± 0.4	9 ± 2
OM97-52	olivine gabbro	525	−2.5 ± 0.2	0.40 ± 0.09	44 ± 12	3.1 ± 0.4	9 ± 1
OM97-45	olivine gabbro	162	−2.1 ± 0.1	0.48 ± 0.05	16 ± 2	4.3 ± 0.6	7.0 ± 2.0
OM97-67a	olivine gabbro	46	−1.7 ± 0.2	0.58 ± 0.09	5 ± 1	4.2 ± 0.7	1.4 ± 0.1

[a]DMTZ, distance from the Moho Transition Zone. See text for definition and computation of CSD parameters (Slope, L_c, Intercept, and L_m) and global parameters (N_v). Errors are 1σ.

larger sizes. In each sample the plagioclase CSD plot was computed for 345–1051 grain sections. At larger grain sizes the bin sizes were adjusted in order to ensure that each bin contains at least four grain section measurements. All these considerations reduce the errors inherent in stereological transformations [*Sahagian and Proussevitch*, 1998; *Higgins*, 2000b]. Two-dimensional and estimated three-dimensional grain size data, together with parameters such as slope and intercept from the CSD plots, are given in Table 1.

[11] The plagioclase CSD plots for our samples are all convex upward, with roughly linear slopes in the larger size range (Figure 5). Convex upward CSD plots similar to Oman gabbros have been documented in plagioclase in different types of plutonic intrusions in the continental crust [*Cashman*, 1990; *Congdon*, 1990; *Heyn et al.*, 1997; *Higgins*, 1998; *Marsh*, 1998; *Higgins*, 2000a]. The linear slope observed for the larger size classes can be produced by a combination of kinetic and/or dynamic factors during igneous crystallization [*Marsh*, 1998]. The change in slope observed for the smallest grain size intervals in the CSD plots may be due to inhibition of nucleation during the last stages of primary crystallization [*Marsh*, 1998] or to processes such as resorption of small crystals [*Marsh*, 1998] and grain growth [*Cashman and Ferry*, 1988; *Higgins*, 1998]. It is not possible to discriminate between the effects of these different processes on the basis of the shape of the CSD plot alone [*Marsh*, 1998; *Higgins*, 2000b].

[12] The slope (mm^{-1}) and intercept (mm^{-4}) of the CSD plots, the maximum crystal size (L_m, mm) [*Marsh*, 1998], and the total number of plagioclase crystals per unit volume of plagioclase (N_V, mm^{-3}) [*Brandeis and Jaupart*, 1987a, 1987b; *Toramaru*, 1991; *Cashman*, 1993] can be related to kinetics and/or dynamic conditions during solidification of igneous rocks. As shown in Figure 6, there is a marked change in the CSD slope, CSD intercept, L_m, and N_V at ∼2 km above the MTZ in the Oman

crustal section we studied. Gabbros <2 km above the MTZ display lower slopes (L_c is the characteristic length in mm and equals -1/slope; $0.39 \leq L_c \leq 0.78$) and smaller L_m ($3.3 \leq L_m \leq 6.7$, mm) and intercepts ($5 \leq$ intercept ≤ 45, mm^{-4}) than gabbros more than 2 km above the MTZ. An exception is sample OM95-75 in the lower half of the gabbro section, which has CSD parameters comparable to gabbros in the upper half of the section (Figure 6).

[13] The ANOVA analysis [e.g., *Davis*, 1986] indicates that the differences between the means of the upper and lower half of the gabbro section for these textural parameters are statistically significant (Table 2). Therefore the mean values of CSD parameters are statistically different for the upper half of the gabbro section compared to the lower half. However, this observation does not directly address the question of whether the change in CSD parameters with height is gradual or whether there is an abrupt change. Scatter in the individual sample values, in both the upper and lower halves of the section, obscures the answer to this question. To address this, in Figure 6 we also show the value of a three-point running average versus height in the section for each of the CSD parameters. The running average values for CSD slope, intercept, L_m, and N_v are nearly constant in the top 1500 m of the gabbro section. Then there is a transitional region between 1500 and 2500 m above the MTZ. Below this transitional region the running average values for CSD slope, intercept, L_m, and N_v are nearly constant in the lower 1500 m of the gabbro section and distinctly different from the upper 1500 m. Thus we conclude that the change in CSD parameters with height is not gradual over the entire section, but instead undergoes a marked change within the interval from 1500 to 2500 m above the MTZ.

[14] It remains for us to determine whether the change in CSD parameters within the interval from 1500 to 2500 m is, itself, gradual with height in the section or more abrupt. Inspection of the data in this specific range of depth reveals a marked difference in values above and below 2000 m. We conclude that the gradational transition observed in the running average values is the result of the smoothing in the averages and that the textural transition in the interval from 1500 to 2500 m is, in fact, sharp and located at ~2000 m.

[15] To evaluate if variations of CSD parameters with depth are due to modal variations of plagioclase, we also investigated possible correlations between plagioclase CSD parameters and the modal proportion of plagioclase in the rock. It is conceivable that "grain boundary pinning" limits the size of plagioclase in rocks with a high proportion of mafic minerals relative to the size in rocks with a high proportion of plagioclase [*Weygand et al.*, 1999; *Evans et al.*, 2001]. Although the mode of the samples discussed up to this point is relatively constant (Figure 2), the effects of grain boundary pinning may be important because some samples are modally banded, with plagioclase-rich layers, while others are not.

[16] To investigate this possibility, we selected specific areas in two banded samples, one sample located >2 km (OM97-100) and the other <2 km above the MTZ (OM97-58), that were particularly rich or poor in plagioclase (Figure 7a) and performed additional CSD analyses on the plagioclase-rich areas. As shown in Figure 7b, our results suggest that the modal proportion of plagioclase has an effect on plagioclase CSD parameters. In both groups of gabbros, >2 km and <2 km above the MTZ, the most plagioclase-rich areas have the largest plagioclase L_m and L_c values. However, this is not the main cause of the bimodal distribution of CSD parameters in our samples. With one exception (OM97-75), at a given plagioclase proportion, samples from the lower

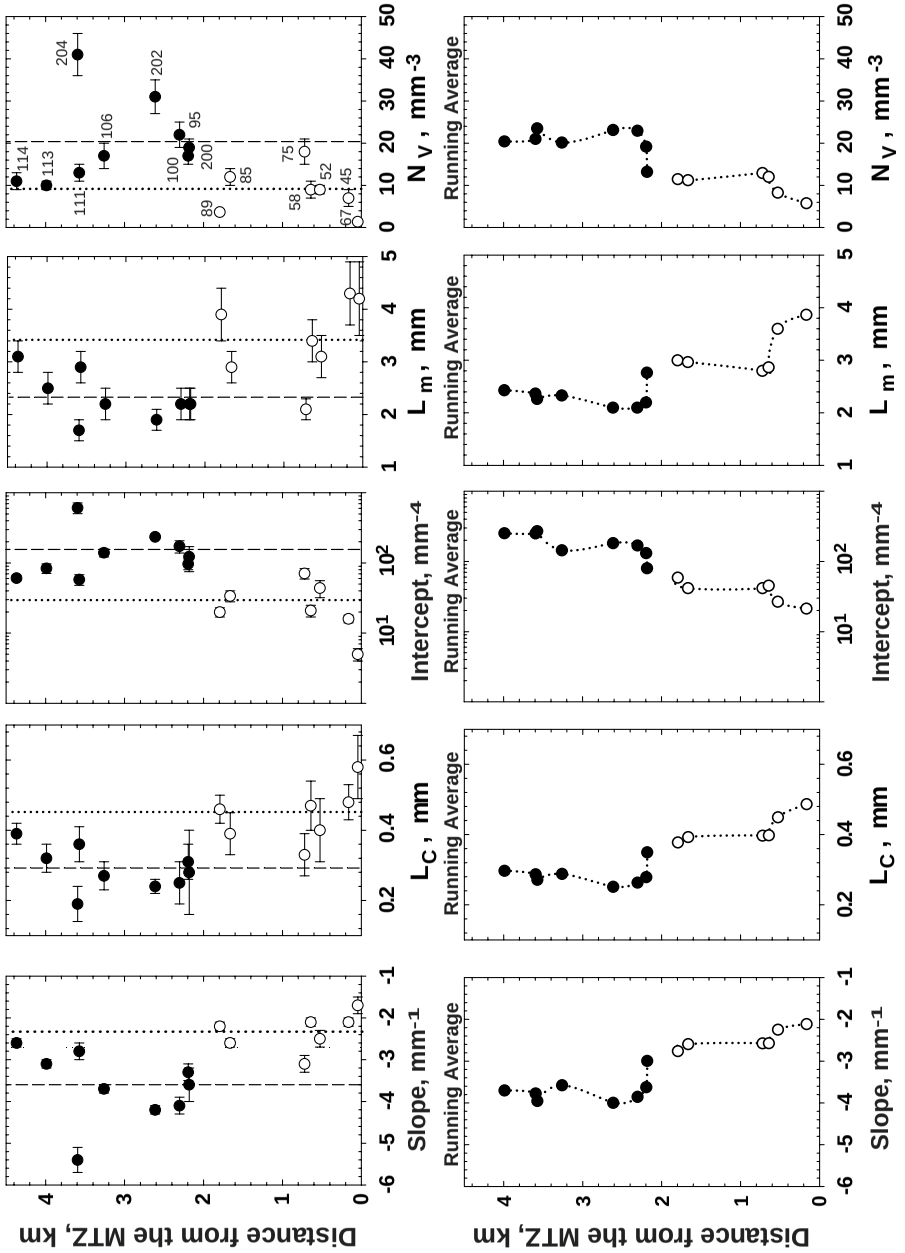
Distance from the MTZ, km
Slope, mm-1
Lc, mm
Intercept, mm-4
Lm, mm
NV, mm-3
Running Average
204
202
114
113
111
106
100
95
200
89
85
75
58
52
67
45

Table 2. Results of the ANOVA Analysis of the Significance of the Variation of Means of CSD Parameter Between Gabbros >2 km and <2 km from the Moho Transition Zone[a]

Parameter	ANOVA		Post-Hoc Tests		Mean	
	F	p	$(L-U)$	S.E.	L	U
Slope, mm^{-1}	18.1	0.001	−1.2	0.3	−2.3	−3.4
L_c, mm	16.0	0.001	−0.15	0.04	0.44	0.29
Intercept, mm^{-4}	17.6	0.001	69	16	10	79
L_m, mm	7.0	0.019	−0.8	0.3	3.1	2.3
N_v pg, mm^{-3}	17.8	0.001	13	3	3	17

[a]ANOVA: analysis of the variance of several CSD parameters to determine the significance of apparent differences between the means of gabbro populations >2 km (n = 9) and <2 km (n = 7) above the MTZ. The F ratio [*Davis*, 1986] is >1 for all investigated CSD parameters, indicating that the means belong to two different populations. The low p values [*Davis*, 1986] indicate that the null hypothesis (null hypothesis is the mean of both groups of gabbros is the same) can be rejected with a confidence level >99% for all CSD parameters except L_m. For L_m, the null hypothesis can be rejected with a confidence level of 98%. Post-hoc test: Result of the LSD post-hoc test [*Davis*, 1986] to estimate the minimum differences between the predicted mean values of CSD parameters between gabbros <2 km and >2 km above the MTZ and their standard error. Mean: Predicted means of CSD parameters for the population of gabbros <2 km (L) and >2 km (U) above the MTZ. All computations were done in DataDesk®.

half of the section have larger L_m and L_c than samples from the upper half (Figure 7b).

4. Discussion

[17] The nearly constant composition of Oman gabbros from just above the MTZ to ~1 km below the base of the sheeted dikes in our sample section (Figure 2) suggests that melt compositions and temperatures of igneous crystallization did not vary significantly. Therefore we conclude that the variation of plagioclase CSD parameters must reflect a difference in kinetic and/or dynamic factors governing gabbro crystallization above and below a boundary located ~2 km from the MTZ. In the following paragraphs we discuss what factors may be important in interpreting these data.

4.1. Plagioclase CSDs in Terms of Igneous Crystallization

[18] Oman gabbro plagioclase CSDs could be interpreted as the result of initial, igneous crys-

Figure 6. Variation of plagioclase CSD parameters as a function of distance from the Moho Transition Zone (MTZ). The slope (mm^{-1}) and intercept (mm^{-4}) of each sample were derived from variance-weighted linear regression of the linear portions of plagioclase CSD plots shown in Figure 5, with 2σ error bars. The characteristic length, L_c (mm), is −1/slope from the CSD plots. L_m is the width of the largest size class, adjusted to contain at least four grains; the error bar on this parameter is equivalent to the width of the largest class. N_v (mm^{-3}) is the number of plagioclase crystals per unit volume of plagioclase in the sample, computed from numerical integration of the 3-D CSD and normalized to the modal proportion of plagioclase in the sample. Solid and open symbols represent gabbro samples >2 km and <2 km above the MTZ, respectively. Vertical dotted and dashed lines indicate the mean values for the population of gabbros <2 km and >2 km above the MTZ. Below each panel we show a three-point running average of the data. The running average values for CSD slope, intercept, and N_V are nearly constant in the top 1500 m of the gabbro section. Then there is a transitional region between 1500 and 2500 m above the MTZ. Below this transitional region the running average values for CSD slope, intercept, and N_V are nearly constant in the lower 1500 m of the gabbro section and distinctly different from the upper 1500 m. Inspection of the data for individual samples in the depth range from 1500 to 2500 m reveals an abrupt change in values above and below 2000 m.

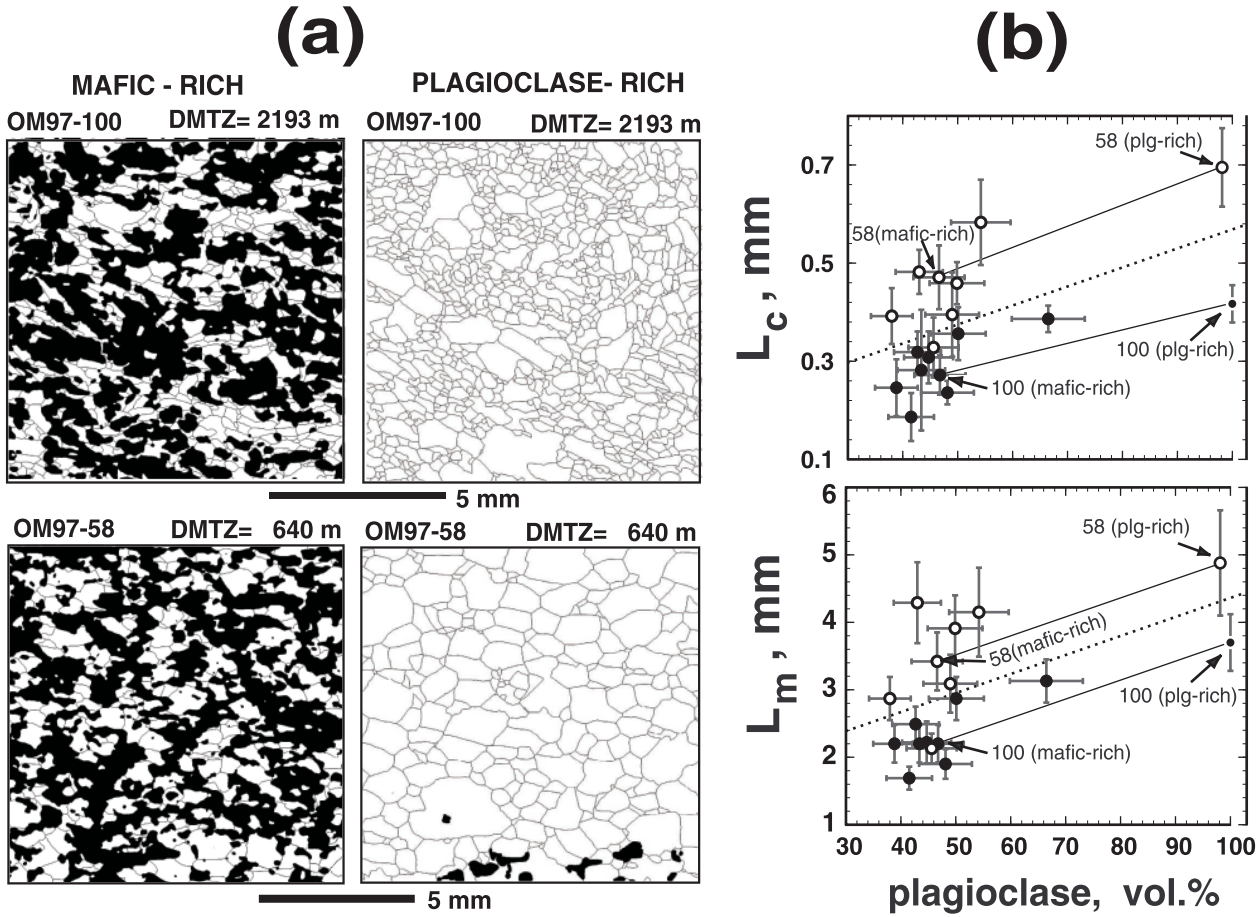

Figure 7. (a) Digital images of the plagioclase grain boundaries (thin lines; clinopyroxene and olivine are black areas) displaying plagioclase-poor regions (left panel) and plagioclase-rich regions (right panel) in one gabbro sample >2 km above the MTZ (above; OM97-100) and another sample <2 km above the MTZ (below; OM97-58). (b) Plots of plagioclase proportion (in vol %) versus characteristic crystal size (L_c, mm) and maximum crystal size (L_m, mm). In each plot, tie lines link L_c and L_m for plagioclase-poor and -rich areas of the same sample. Samples from the lower half of the gabbro section are indicated by open circles, while those from the upper half are shown as solid circles. The dashed line separates the regions where most samples are located either >2 km or <2 km from the MTZ.

tallization, recorded by the straight segment of the CSD plot, followed by late stage dissolution of the smaller crystals and/or subsolidus grain growth [*Cashman and Ferry*, 1988; *Cashman and Marsh*, 1988; *Marsh*, 1988, 1998]. Two end-member igneous scenarios can produce a CSD plot with the shape shown by our samples: (1) single-stage, closed-system crystallization (termed ''batch crystallization'' by *Marsh* [1998]) or (2) open-system, steady state crystallization [*Marsh*, 1998]. Note that in this context, ''open'' and ''closed'' refer to the transport of crystals into and out of a particular crystallizing magma body. They do not indicate whether the system was closed to chemical transfer. The plagioclase CSDs and the major and trace element composition of Oman gabbros are consistent with either scenario.

[19] In closed-system crystallization, $\log_e$-linear CSD plots can be produced if the crystal nucleation rate increases exponentially and the effective crystal growth rate is constant. In general, during the initial stages of crystallization, the crystal nucleation rate dN/dt is proportional to $\exp(-1/dT^2)$, where dT is the difference between the liquidus temperature and the ambient temperature [e.g., *Kingery*, 1960; *Lasaga*, 1998]. Thus the more rapid the cooling, the faster the exponential increase of the nucleation rate, and the steeper the slope of the CSD. Hence variation in the slope for compositionally similar samples such as our Oman gabbros may reflect sample-to-sample variation in cooling rates during crystallization [*Cashman and Marsh*, 1988; *Cashman*, 1990, 1993; *Marsh*, 1998].

[20] Alternatively, the $\log_e$-linear portion of the CSDs can be produced if the growth rate increases exponentially with crystal size and nucleation rate is constant [*Marsh*, 1998]. However, we have not considered this possibility because it is not clear why the growth rate would increase exponentially with size, and there is no observational or experimental evidence that the nucleation rate can remain constant or decrease during closed-system cooling and crystallization of plutonic rocks [*Cashman*, 1990, 1993; *Marsh*, 1998].

[21] In open-system, steady state crystallization, $\log_e$-linear CSDs can be produced via systematic variation in the influx and outflow of crystals from magma reservoirs, such that the mean residence time of crystals is different in different reservoirs [*Marsh*, 1988, 1998]. At steady state the reciprocal of the CSD slope is equal to the product of the growth rate and the mean residence time of crystals in the reservoir [*Marsh*, 1988, 1998]. In this case the distribution of slopes observed in Oman samples would reflect sample-to-sample variation in the mean residence time of crystals in an open magmatic reservoir. This might give rise to an abrupt change in CSD characteristics between the upper and lower halves of the gabbroic section (Figure 6; Table 2) if the gabbros crystallized in two different magmatic reservoirs under different ''steady'' conditions of crystallization.

[22] Correlations between CSD parameters for different samples crystallized from similar magmas can be diagnostic of crystallization processes [*Marsh*, 1998]. The slopes of plagioclase CSDs in the Oman section correlate with plagioclase L_m and with plagioclase CSD intercepts, while L_m is negatively correlated with intercepts (Figure 8). Similar correlations of plagioclase CSD parameters are observed in gabbros from the Peneplain sill intrusion (Antarctica) [*Heyn et al.*, 1997; *Marsh*, 1998] and plagioclase phenocryst-rich lavas from Atka (Aleutian Islands, Alaska) [*Resmini and Marsh*, 1995; *Marsh*, 1998]. In open-system, steady state crystallization, the slope of the CSD is not necessarily related to the intercept [*Marsh*, 1998]. Thus the correlation between slope and intercept implies that Oman gabbros did not

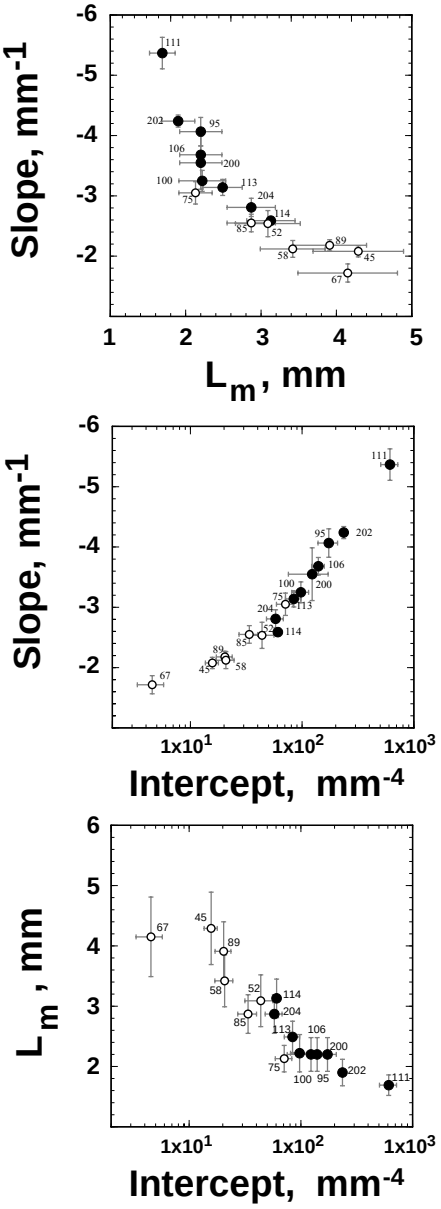

Figure 8. Correlation between plagioclase CSD parameters in Oman gabbro samples. Solid and open symbols represent gabbro samples located >2 km and <2 km above the MTZ, respectively.

form via open-system, steady state crystallization, and instead formed via a mechanism approaching closed-system, single-stage crystallization [*Marsh*, 1998].

[23] Finally, mechanical processes in magma chambers, such as crystal removal or accumulation, could change plagioclase CSDs [*Marsh*, 1988, 1998; *Cashman*, 1990]. However, simple crystal removal and/or accumulation processes lead to kinked CSD plots [*Marsh*, 1998] with shapes that we do not observe in Oman gabbros.

[24] If the linear portion of the CSDs arises as a result of igneous crystallization, we conclude that the marked change in CSD parameters with depth implies faster cooling during crystallization of gabbros from >2 km above the MTZ than for gabbros <2 km above the MTZ. This interpretation of CSD parameters is supported by the variation in N_v (Figure 6), which is also predicted to be dependent on igneous cooling rate [*Brandeis et al.*, 1984; *Brandeis and Jaupart*, 1987a; *Toramaru*, 1991; *Cashman*, 1993].

4.2. Role of Postcrystallization Grain Growth

[25] The spatial distribution of CSDs could also be the result of crystal dissolution and/or grain growth, either in a "crystal mush" or during later, subsolidus processes. *Higgins* [1998, 2000a] argued that coarsening processes decrease the slope of the linear portion of CSD plots. In contrast, others have suggested that crystal resorption and isothermal coarsening do not modify the slope of the linear portion of CSD plots [*Cashman and Ferry*, 1988; *Marsh*, 1988, 1998; *Cashman*, 1990]. This discrepancy may arise, at least in part, from extrapolation of coarsening theories from dilute solutions to the dense crystal mushes that must have been present during the last stages of solidification of plutonic rocks [*Higgins*, 1998]. This is a topic of current debate in the material science literature [*DeHoff*, 1991; *Marsh and Glicksman*, 1996]. However, our understanding is that grain growth processes tend to broaden the width of the grain size distribution [*Atkin-*

son, 1988], thereby decreasing the slope of CSD plots for large grain sizes.

[26] If the initial CSDs of Oman gabbros <2 km above the MTZ were similar to those now observed in gabbros >2 km above the MTZ, enhanced coarsening of the lowermost gabbros could explain the correlations of CSD parameters observed in our data (Figure 8). Coarsening would also account for the lower values of N_v in gabbros <2 km above the MTZ (Figure 6). In this interpretation the enhanced coarsening of gabbros <2 km above the MTZ implies slower cooling for these samples compared with those >2 km above the MTZ.

[27] So far, we have discussed grain growth as though plagioclase CSDs in Oman gabbros result from a single stage of igneous crystallization and subsequent cooling. However, data on heat flow in oceanic crust show that the crust is first cooled by hydrothermal convection, and then parts of the crust reheat during conductive reequilibration. It is thus necessary to ask whether some grain growth could have occurred during this later reheating. The heat flow data are consistent with reheating that is complete ~5 Myr after crustal formation [e.g., *Stein and Stein*, 1994], at which time the temperature at the base of the crust along a conductive geotherm would be <500°C. Experimentally determined grain growth kinetics for plagioclase [*Dresen et al.*, 1996] indicate that growth rates are negligible at temperatures <500°C. For example, with an initial grain size of 1 mm the grain size would increase by only ~2 nm in 100 million years. Therefore our assumption that plagioclase CSDs in Oman gabbros were produced by igneous processes is well-founded.

4.3. Implications and Conclusions

[28] To first order, our data indicate that there must have been an abrupt change in cooling rate as a function of depth within the Khafifah crustal section. This is true whether the observed systematics in CSD parameters result from igneous crystallization or subsequent coarsening. An abrupt change in cooling rates as a function of depth within the plutonic section of the oceanic crust is inconsistent with most current models for cooling of crust at mid-ocean ridges [*Sleep*, 1975; *Phipps Morgan and Chen*, 1993; *Chen and Morgan*, 1996; *Chevenez et al.*, 1998]. In these models the effects of hydrothermal convection are approximated by using a single, enhanced thermal conductivity together with a purely conductive heat transport mechanism. Such an approach cannot account for locally varying, advective heat transport resulting from spatial variation of convective vigor and instead must give rise to isotherms with a shape controlled by thermal diffusion. This, in turn, leads to smooth variations in predicted cooling rates as a function of depth in the crustal section.

[29] Our results are, however, consistent with the results of a recent seismic tomography study of the oceanic crust beneath the East Pacific Rise near 9°30′N. *Dunn et al.* [2000] observe that the lower crustal, seismic velocity anomaly associated with high temperatures and/or the presence of melt is very narrow with steep sides. They suggested that the derived thermal structure implies efficient hydrothermal cooling throughout the oceanic crust.

[30] *Dunn et al.* [2000] infer that the zone with detectable melt present is about 4–8 km wide (full width) >2 km above the MTZ, widening to 8–12 km <2 km above the MTZ. If variations in plagioclase CSD parameters in the Oman crustal section are the result of single-stage, closed-system crystallization, the size of the largest crystals in the system (L_m) can be used together with the "effective growth rate" (G_o) to estimate the crystallization time (t_c), since $t_c = L_m/G_o$ [*Marsh*, 1998]. Assuming a constant value for G_o [*Cashman*, 1993; *Marsh*, 1998], the observed difference in L_m between the two

populations of gabbros in our crustal section (Table 2) indicates that the upper 2 km of gabbro crystallized ~1.5 times faster, on average, than the lower 2 km of gabbro, with a maximum of 2.7 times faster for sample OM97-111 compared with lowermost gabbro samples.

[31] We can now compare our results to the seismic data. Cooling of lower crustal rocks beneath a medium- to fast-spreading ridge occurs as the crust is transported laterally away from the ridge, crossing isotherms. If gabbro from the upper half of the section completely crystallized over a width of 4–8 km, as suggested by the data from the East Pacific Rise, gabbros from the lower half of the section should have completely crystallized over a region 1.5 times wider, i.e., 6–12 km wide. In detail the largest L_m are found in gabbros just above the MTZ (Figure 6), and the reasoning in the previous paragraph suggests that these cooled over a region twice as wide as the shallowest gabbros, i.e., 8–16 km wide.

[32] Our results are also consistent with recent modeling of hydrothermal circulation in the crust surrounding mid-ocean ridges by *Cherkaoui et al.* [1999]. Assuming that (1) permeability and the physical properties of fluid are constant throughout the oceanic crust, (2) magma input is restricted to a narrow region immediately below the ridge, and (3) heat input from the underlying mantle decreases smoothly away from the ridge axis, then hydrothermal convection would occur throughout the oceanic crust, producing strong upwelling with nearly vertical flow lines and isotherms near the ridge axis. Of course, the permeability structure of oceanic crust is not so simple. However, *Cherkaoui et al.* [1999] quantified this scenario, and then evaluated the effects of (1) different permeability structures and (2) a realistic equation of state for aqueous fluids. In all cases their models predicted rapid hydrothermal convection extending well into the lower crust.

[33] A simple illustration of the possible thermal structure and igneous accretion of the oceanic crust based on our data is shown in Figure 9. Hydrothermal convection can remove heat effectively down to the middle of the lower crust. Such convection would enhance the rates of cooling and igneous crystallization, modifying the slope of lower crustal isotherms. Some convection cells may be "sealed," with little chemical exchange with the overlying volcanic section and seawater. Closed cells would recycle fluid that has already equilibrated with lower crustal gabbros, preserving a relatively low geochemical water/rock ratio.

[34] Some reviewers of the submitted version of this manuscript believed that Figure 9, with its multiple magma lenses at a variety of depths in the crust, is inconsistent with seismic data from the East Pacific Rise (EPR). This may arise as a result of the overly restrictive interpretation of seismic data. It is clear that there is a steady state, "shallow melt lens" 1–3 km wide and a few hundred meters high, at a depth of 1–2 km beneath the ridge axis for much of the length of the EPR [e.g., *Detrick et al.*, 1987; *Vera et al.*, 1990; *Kent et al.*, 1993, 1994]. In our Figure 9 this is represented as the shallowest of several melt lenses in the crust.

[35] However, the structure beneath the shallow melt lens is not well defined. Conventional refraction and tomographic studies [e.g., *Vera et al.*, 1990; *Wilcock et al.*, 1995; *Dunn et al.*, 2000] indicate that there is a low velocity zone a few kilometers wide beneath the "melt lens" extending below to the base of the crust. This zone is largely shielded from seismic reflection studies by the shallow melt lens, so it is uncertain whether it is uniform or, for example, layered. Because the magnitude of the low-velocity anomaly, relative to older crust off axis, is larger than can be accounted for by temperature variation, it

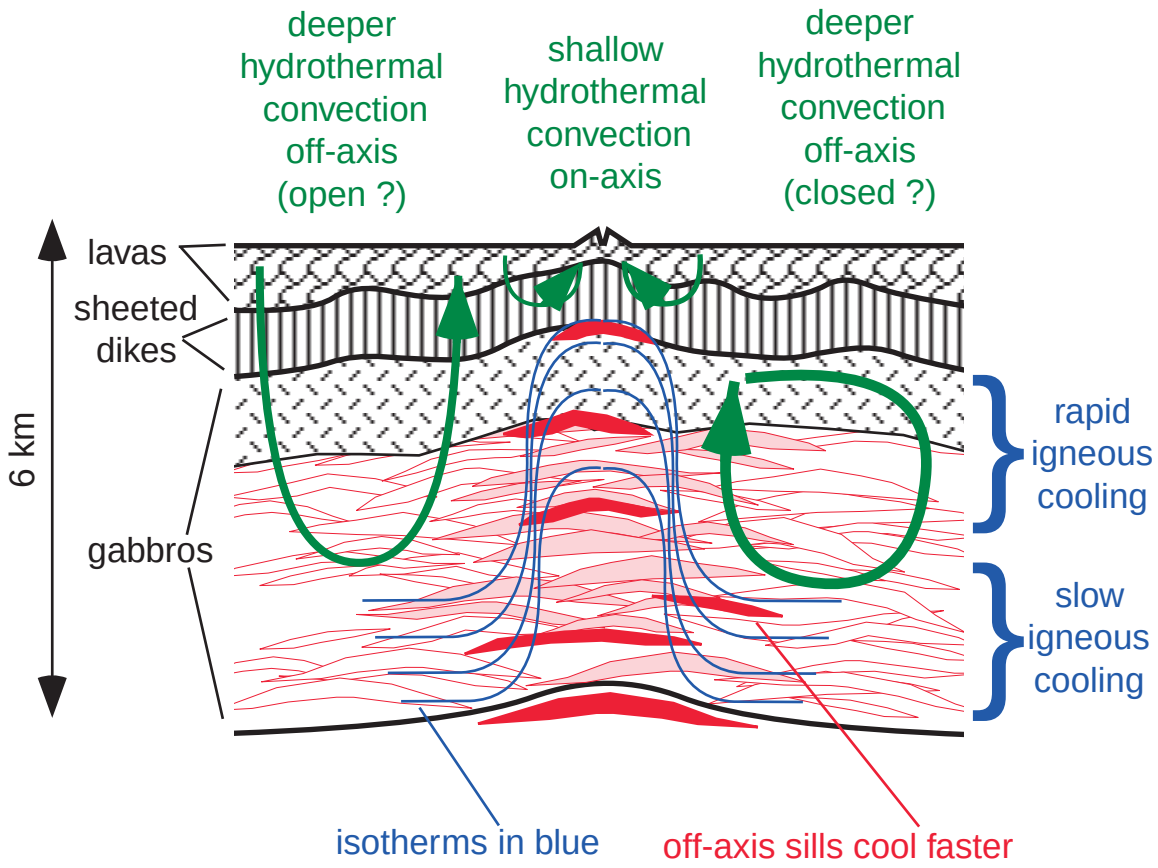

Figure 9. Illustration of thermal structure and accretion of the oceanic crust at medium- to fast-spreading oceanic ridges consistent with our CSD data. Green curved arrows indicate two different hydrothermal convection systems. A shallow, on-axis system extends to the base of the sheeted dikes. A deeper, off-axis system effectively removes heat from the uppermost 2 km of the plutonic crust, leading to closely spaced, near-vertical isotherms (blue curved lines) and faster cooling of shallow gabbros. Near the base of the crust, isotherms are nearly horizontal, and gabbros cool much more slowly. In our preferred model, crustal accretion is accommodated throughout the crust by the intrusion of gabbro sills at different depths.

apparently requires the presence of melt in the lower crust. For simplicity, the data are often interpreted in terms of a melt fraction or "porosity". However, this is based on the assumption that melt is homogeneously distributed, for example, in a grain boundary network.

[36] It is clear that the seismic data could also be modeled as the result of melt lenses at the meter to 100 m length scale within rock containing little or no melt. In fact, analyses of compliance beneath the EPR at ~9°N indicate that there is a large melt lens at Moho depths, in addition to the shallow melt lens. Another indication that melt is not homogeneously distributed in an interconnected grain boundary network comes from analysis of lower gabbros in the Oman ophiolite. The spatial variation of mineral compositions in these gabbros is inconsistent with diffuse, porous flow of melt through the section [*Korenaga and Kelemen*,

1998]. In one case, variation of Fe/Mg in olivine on a centimeter scale suggests that there was no interconnected grain boundary melt network in the gabbros after their initial crystallization, even on this short length scale [*Korenaga and Kelemen*, 1997].

[37] A recent study of gabbros in the Al Abyad section of Nakhl massif of the Oman ophiolite suggests that approximately the upper 40% of the gabbroic, lower crustal section formed via ductile flow of a crystal mush downward and outward, after crystallization in a "shallow melt lens." This interpretation was based on textural and chemical divisions of the gabbros [*MacLeod and Yaouancq*, 2000]. However, the Khafifah section of the Wadi Tayin massif, studied here, is different from the Al Abyad section. As documented by *Pallister and Hopson* [1981], there is a substantial textural and chemical break between (1) foliated and varitextured, incompatible element rich "upper gabbros" and (2) modally layered, incompatible element depleted "lower gabbros" in the Khafifah section. This break occurs ~3500 m above the MTZ, with upper gabbros occupying the upper 1000 m, or 22%, of the lower crustal section. This break is clearly evident in our Figure 2. In our Figure 9 these upper gabbros are indicated with a hachured pattern. Thus, if *MacLeod and Yaouancq* [2000] are correct in their interpretation that upper gabbros formed from a shallow melt lens while lower gabbros formed from a series of sills, only the upper 22% of the Khafifah section formed from a shallow melt lens.

[38] In summary, on the basis of the data in this paper and previous results [*Boudier et al.*, 1996; *Kelemen et al.*, 1997; *Korenaga and Kelemen*, 1997, 1998; *Kelemen and Aharonov*, 1998], we favor a model for igneous crustal accretion in which gabbros crystallize on-axis in sills distributed in at least two different crustal levels and crystallizing in two distinct cooling regimes. The upper half of the gabbroic section is transported rapidly across vertical isotherms into the zone of active hydrothermal convection and so cools rapidly. In contrast, seafloor spreading moves the lower half of the plutonic section across a region beneath the active hydrothermal system, characterized by nearly horizontal isotherms, resulting in much slower cooling. Some gabbros may crystallize slightly off-axis (e.g., sample OM97-75), undergoing faster crystallization and yielding a second-order source of "noise" in the observed pattern of CSDs with depth in the crustal section. We anticipate that the details of this scenario, particularly the maximum depth of vigorous hydrothermal circulation, must vary substantially from place to place, even where spreading rate and crustal thickness are nearly constant. Thus we wish to emphasize only the most general features of this hypothesis.

Acknowledgments

[39] We thank Jim Natland, Jackie Dixon, Bill White, and an anonymous reviewer for their helpful and (in Natland's case) entertaining comments on the submitted manuscript. We are indebted to Michael Braun and Shannon McDaniel for field assistance, sample preparation, and help obtaining the digital images. We are grateful to Peter Meyer for numerous discussions and for bringing our attention to the potential of CSDs for the study of oceanic gabbros. We thank Tony Peterson, Alexis Proussevitch, and Kathy Cashman for thoughtful advice on obtaining and interpreting CSDs. Michael Higgins generously provided us with unpublished work and software to assist in the interpretation of CSDs. This research was possible thanks to NSF grants OCE-9416616, OCE-9711170, and OCE-9819666.

References

Atkinson, H. V., Theories of normal grain growth in pure single phase systems, *Acta Metall.*, *36*(3), 469–491, 1988.

Boudier, F., A. Nicolas, and B. Ildefonse, Magma chambers in the Oman Ophiolite: Fed from the top and the bottom?, *Earth Planet. Sci. Lett.*, *144*(1-2), 239–250, 1996.

Brandeis, G., and C. Jaupart, Crystal sizes in intrusions of different dimensions: Constraints on the cooling regime and the crystallization kinetics, in *Magmatic Processes: Physicochemical Principles*, edited by B. O. Mysen, pp. 307–318, Geochem. Soc., University Park, Pa., 1987a.

Brandeis, G., and C. Jaupart, The kinetics of nucleation and crystal growth and scaling laws for magmatic crystallization, *Contrib. Mineral. Petrol.*, *96*, 24–34, 1987b.

Brandeis, G., C. Jaupart, and C. J. Allègre, Nucleation, crystal growth and the thermal regime of cooling magmas, *J. Geophys. Res.*, *89*, 10,161–10,177, 1984.

Cashman, K. V., Textural constraints on the kinetic of crystallization of igneous rocks, in *Modern Methods of Igneous Petrology: Understanding Magmatic Processes*, edited by J. Nicholls and J. K. Russell, pp. 260–314, Mineral. Soc. of Am., Washington, D. C., 1990.

Cashman, K. V., Relationship between plagioclase crystallization and cooling rate in basaltic melts, *Contrib. Mineral. Petrol.*, *113*(1), 126–142, 1993.

Cashman, K. V., and J. M. Ferry, Crystal size distribution (CSD) in rocks and the kinetics and dynamics of crystallization, III, Metamorphic crystallization, *Contrib. Mineral. Petrol.*, *99*, 401–415, 1988.

Cashman, K. V., and B. D. Marsh, Crystal size distribution (CSD) in rocks and the kinetics and dynamics of crystallization, II, Makaopuhi lava lake, *Contrib. Mineral. Petrol.*, *99*, 292–305, 1988.

Chen, Y. J., and J. P. Morgan, The effects of spreading rate, the magma budget, and the geometry of magma emplacement on the axial heat flux at mid-ocean ridges, *J. Geophys. Res.*, *101*(B5), 11,475–11,482, 1996.

Cherkaoui, A. S. M., A. R. Dunn, W. S. D. Wilcock, and D. R. Toomey, Numerical models of hydrothermal cooling of the lower crust on the East Pacific Rise: Thermal constraints from seismic tomography, *Eos Trans. AGU*, *80*(46), Fall Meet. Suppl., F1048, 1999.

Chevenez, J., P. Machetel, and A. Nicolas, Numerical models of magma chambers in the Oman ophiolite, *J. Geophys. Res.*, *103*, 15,443–15,455, 1998.

Congdon, R. D., The solidification of the Shokin Sag Laccolith: Mineralogy, petrology, and experimental phase equilibria, Ph.D. dissertation, Johns Hopkins Univ., Baltimore, Md., 1990.

Davis, J. C., *Statistics and Data Analysis in Geology*, 2nd ed., 646 pp, John Wiley, New York, 1986.

DeHoff, R. T., A geometrically general theory of diffusion controlled coarsening, *Acta Metall. Mater.*, *39*(10), 2349–2360, 1991.

Detrick, R. S., P. Buhl, E. Vera, J. Mutter, J. Orcutt, J. Madsen, and T. Brocher, Multi-channel seismic imaging of a crustal magma chamber along the East Pacific Rise, *Nature*, *326*, 35–41, 1987.

Dresen, G., Z.-C. Wang, and Q. Bai, Kinetics of grain growth in anorthite, *Tectonophysics*, *258*, 251–262, 1996.

Dunn, R. A., D. R. Toomey, and S. C. Solomon, Three-dimensional seismic structure and physical properties of the crust and shallow mantle beneath the East Pacific Rise at 9°30′, *J. Geophys. Res.*, *105*(B10), 23,557–23,568, 2000.

Evans, B., J. Renner, and G. Hirth, A few remarks on the kinetics of static grain growth in rocks, *Int. J. Earth Sci.*, *90*(1), 88–103, 2001.

Heyn, J., B. D. Marsh, and M. M. Wheelock, Crystal size and cooling time in the Peneplain sill, Dry Valley Region, Antarctica, *Antarct. J. U. S.*, *30*, 50–51, 1997.

Higgins, M. D., Numerical modeling of crystal shapes in thin sections: Estimation of crystal habit and true size, *Am. Mineral.*, *79*, 113–119, 1994.

Higgins, M. D., Origin of anorthosite by textural coarsening: Quantitative measurements of a natural sequence of textural development, *J. Petrol.*, *39*, 1307–1323, 1998.

Higgins, M., Origin of megacrysts in granitoids by textural coarsening: A crystal size distribution (CSD) study of microcline in the Cathedral Peak Grandiorite, Sierra Nevada, California, in *Understanding Granites: Integrating Modern and Classical Techniques*, edited by C. Fernandez and A. Castro, *Geol. Soc. Spec. Publ.*, 207–219, 2000a.

Higgins, M. D., Measurement of crystal size distributions, *Am. Mineral.*, *85*(9), 1105–1116, 2000b.

Hopson, C. A., R. G. Coleman, R. T. Gregory, J. S. Pallister, and E. H. Bailey, Geologic section through the Samail ophiolite and associated rocks along a Muscat-Ibra transect, southeastern Oman Mountains, edited by R. G. Coleman and C A. Hopson, *J. Geophys. Res.*, *86*, 2527–2544, 1981.

Kelemen, P. B., and E. Aharonov, Periodic formation of magma fractures and generation of layered gabbros in the lower crust beneath oceanic spreading ridges, in *Faulting and Magmatism at Mid-Ocean Ridges*, *Geophys. Monogr. Ser.*, vol. 106, edited by W. R. Buck et al, pp. 267–289, AGU, Washington, D. C., 1998.

Kelemen, P. B., K. Koga, and N. Shimizu, Geochemistry of gabbro sills in the crust-mantle transition zone of the Oman Ophiolite: Implications for the origin of the oceanic lower crust, *Earth Planet. Sci. Lett.*, *146*(3-4), 475–488, 1997.

Kent, G. M., A. M. Harding, and J. A. Orcutt, Distribution of magma beneath the East Pacific Rise between the Clipperton Transform and the 9°17′N deval from forward modeling of common depth point data, *J. Geophys. Res.*, *98*(8), 13,945–13,969, 1993.

Kent, G. M., A. J. Harding, J. A. Orcutt, R. S. Detrick, J. C. Mutter, and P. Buhl, Uniform accretion of oceanic crust south of the Garrett Transform at 14°15′S on the

East Pacific Rise, *J. Geophys. Res.*, *99*(5), 9097–9116, 1994.

Kingery, W. D., *Introduction to Ceramics*, 781 pp., John Wiley, New York, 1960.

Korenaga, J., and P. B. Kelemen, The origin of gabbro sills in the Moho transition zone of the Oman ophiolite: Implications for magma transport in the oceanic lower crust, *J. Geophys. Res.*, *102*, 27,729–27,749, 1997.

Korenaga, J., and P. B. Kelemen, Melt migration through the oceanic lower crust: A constraint from melt percolation modeling with finite solid diffusion, *Earth Planet. Sci. Lett.*, *156*(1–2), 1–11, 1998.

Lasaga, A. C., *Kinetic Theory in Earth Sciences*, 811 pp., Princeton Univ. Press, Princeton, N. J., 1998.

MacLeod, C. J., and G. Yaouancq, A fossil melt lens in the Oman ophiolite: Implications for magma chambers processes at fast spreading ridges, *Earth Planet. Sci. Lett.*, *176*, 357–373, 2000.

Marsh, B. D., Crystal size distribution (CSD) in rocks and the kinetics and dynamics of crystallization, I, Theory, *Contrib. Mineral. Petrol.*, *99*, 277–291, 1988.

Marsh, B. D., On the interpretation of crystal size distributions in magmatic systems, *J. Petrol.*, *39*, 553–599, 1998.

Marsh, S. P., and M. E. Glicksman, Kinetics of phase coarsening in dense systems, *Acta Mater.*, *44*(9), 3761–3771, 1996.

Nicolas, A., *Structures of Ophiolites and Dynamics of Oceanic Lithosphere*, 367 pp., Kluwer Acad., Norwell, Mass., 1989.

Nicolas, A., F. Boudier, and B. Ildefonse, Variable crustal thickness in the Oman Ophiolite: Implication for oceanic crust, *J. Geophys. Res.*, *101*(B8), 17,941–17,950, 1996.

Pallister, J. S., and C. A. Hopson, Samail ophiolite plutonic suite: Field relations, phase variation, cryptic variation and layering, and a model of a spreading ridge magma chamber, *J. Geophys. Res.*, *86*, 2593–2644, 1981.

Pallister, J. S., and R. J. Knight, Rare-earth element geochemistry of the Samail ophiolite near Ibra, Oman, *J. Geophys. Res.*, *86*, 2673–2697, 1981.

Pearce, J. A., T. Alabaster, A. W. Shelton, and M. P. Searle, The Oman ophiolite as a Cretaceous arc-basin complex: Evidence and implications, *Philos. Trans. R. Soc. London, Ser. A*, *300*, 299–317, 1981.

Peterson, T. D., A refined technique for measuring crystal size distributions in thin section, *Contrib. Miner. Petrol.*, *124*, 395–405, 1996.

Phipps Morgan, J., and Y. J. Chen, The genesis of oceanic crust: Magma injection, hydrothermal circulation, and crustal flow, *J. Geophys. Res.*, *98*, 6283–6297, 1993.

Resmini, R. G., and B. D. Marsh, Steady-state volcanism, paleoeffusion rates, and magma system volume inferred from plagioclase crystal size distributions in mafic lavas: Dome Mountain, Nevada, *J. Volcanol. Geotherm. Res.*, *68*(4), 273–296, 1995.

Sahagian, D. L., and A. A. Proussevitch, 3D particle size distributions from 2D observations: Stereology for natural applications, *J. Volcanol. Geotherm. Res.*, *84*(3-4), 173–196, 1998.

Sleep, N. H., Formation of oceanic crust: Some thermal constraints, *J. Geophys. Res.*, *80*, 4037–4042, 1975.

Stein, C. A., and S. Stein, Constraints on hydrothermal heat flux through the oceanic lithosphere from global heat flow, *J. Geophys. Res.*, *99*, 3081–3095, 1994.

Toramaru, A., Model of nucleation and growth of crystals in cooling magmas, *Contrib. Mineral. Petrol.*, *108*, 106–117, 1991.

Vera, E. E., J. C. Mutter, P. Buhl, J. A. Orcutt, A. J. Harding, M. E. Kappus, R. S. Detrick, and T. M. Brocher, The structure of 0- to 0.2 m.y.-old oceanic crust at 9°N on the East Pacific Rise from expanded spread profiles, *J. Geophys. Res.*, *95*, 15,529–15,556, 1990.

Weygand, D., Y. Bréchet, and J. Lépinoux, Zener pinning and grain growth: A two dimensional vertex computer simulation, *Acta Mater.*, *47*, 961–970, 1999.

Wilcock, W. S. D., S. C. Solomon, G. M. Purdy, and D. R. Toomey, Seismic attenuation structure of the East Pacific Rise near 9°30′N, *J. Geophys. Res.*, *100*, 24,147–24,165, 1995.